A&A 517, A45 (2010)
DOI: 10.1051/0004-6361/200912817

Astronomy & Astrophysics

From interstellar abundances to grain composition: the major dust constituents Mg, Si, and Fe*

N. V. Voshchinnikov[1,2,3] and Th. Henning[1]

[1] Max-Planck-Institut für Astronomie, Königstuhl 17, 69117 Heidelberg, Germany
e-mail: voshchinnikov@mpia.de
[2] Sobolev Astronomical Institute, St. Petersburg University, Universitetskii prosp. 28, 198504 St. Petersburg, Russia
e-mail: nvv@astro.spbu.ru
[3] Isaac Newton Institute of Chile, St. Petersburg Branch, Russia

Received 3 July 2009 / Accepted 6 April 2010

ABSTRACT

We analyse observational correlations for three elements entering into the composition of interstellar silicate and oxide grains. Using current solar abundances, we converted the gas phase abundances into dust phase abundances for 196 sightlines. We deduce a sharp difference in abundances for sightlines located at low ($|b| < 30°$) and high ($|b| > 30°$) galactic latitudes. For high-latitude stars, the ratios Mg/Si and Fe/Si in dust are close to 1.5. For disk stars they are reduced to Mg/Si $\sim$ 1.2 and Fe/Si $\sim$ 1.05. The derived numbers indicate that 1) the dust grains cannot be the mixture of silicates with olivine and pyroxene composition only, and some amount of magnesium or iron (or both) should be in another population and that 2) the destruction of Mg-rich grains in the warm medium is more effective than for Fe-rich grains. We reveal a decrease in dust phase abundances and correspondingly an increase in gas phase abundances with distance D for stars with $D \gtrsim 400$ pc. We attribute this to an observational selection effect: a systematic trend toward lower observed hydrogen column density for distant stars. We find differences in abundances for disk stars with low ($E(B-V) \lesssim 0.2$) and high ($E(B-V) \gtrsim 0.2$) reddenings that reflect the distinction between the sightlines passing through diffuse and translucent interstellar clouds. For Scorpius-Ophiuchus, we detect a uniform increase in dust phase abundances of Mg and Si with an increase in the ratio of total to selective extinction R_V and a decrease in the strength of the far-UV extinction. This is the first evidence of growth of Mg-Si grains due to accretion in the interstellar medium.

Key words. ISM: abundances – dust, extinction

1. Introduction

Interstellar space is filled with gas and dust. Both components interact with each other. Atoms and molecules collide with solid particles and cause grain growth or destruction (sputtering). It depends on the relative velocity. An examination of these processes is based on analysis of the observed gas phase abundances. Spectroscopic studies of interstellar UV absorption lines started in the 1970s have revealed a deficit of heavy elements in the ISM in comparison with cosmic (solar reference) abundances (Spitzer & Jenkins 1975). The missing atoms were assumed to be tied up in solid particles that opened an indirect way to investigate the element composition of interstellar dust. Modelling of interstellar extinction (e.g., Li & Greenberg 1997; Zubko et al. 2004; Voshchinnikov et al. 2006) has demonstrated that cosmic abundance constraints might be crucial in deciding on modern dust models.

Cosmic abundances of heavy elements obtained from spectroscopic studies of ordinary stars (Snow & Witt 1996; Przybilla et al. 2008) and a decrease in the estimates of metal abundances in the solar atmosphere over the past years (Asplund et al. 2005, 2009) essentially limited the number of atoms incorporated into dust particles. In this situation, accurate determination and analysis of gas phase abundances are especially important.

A quantitative theory of element depletions is lacking. First phenomenological models showed a possible dependence of depletions on the element equilibrium condensation temperature (Field 1974) and the first or second element ionization potential (Snow 1973; Tabak 1979). The dependence of gas phase abundances on hydrogen column density, fraction of molecular hydrogen, distance, location, etc., were also considered (Tarafdar et al. 1983; Harris et al. 1984; Jenkins et al. 1986; see also references in Jensen 2007; and Jenkins 2009).

A fresh approach to the problem of gas phase abundances has been devised by Jenkins (2004, 2009, hereafter J09) who investigated general patterns in depletions of 17 elements. He finds that the propensity of an element X to convert from gas to solid phase can be described by a linear equation with coefficient A_X. The values of A_X are assumed to be the same for all sightlines, while the individual sightlines can be characterized by a depletion factor F_* which is common to all elements. This means that all elements are depleted in unison independently of local physical conditions.

In this paper, we exploit a more traditional approach by trying to keep individual features of separate sightlines. We investigate correlations in abundances of three elements Mg, Si, and Fe, which are classified as *major* dust constituents (Jones 2000). These elements along with the *primary* element O can be incorporated in solid phase in the form of Mg-Fe silicates, metal particles, or oxides. We outline oxygen abundances, which will be fully discussed elsewhere. Another primary element, C,

* Table A.1 is only available in electronic form at http://www.aanda.org

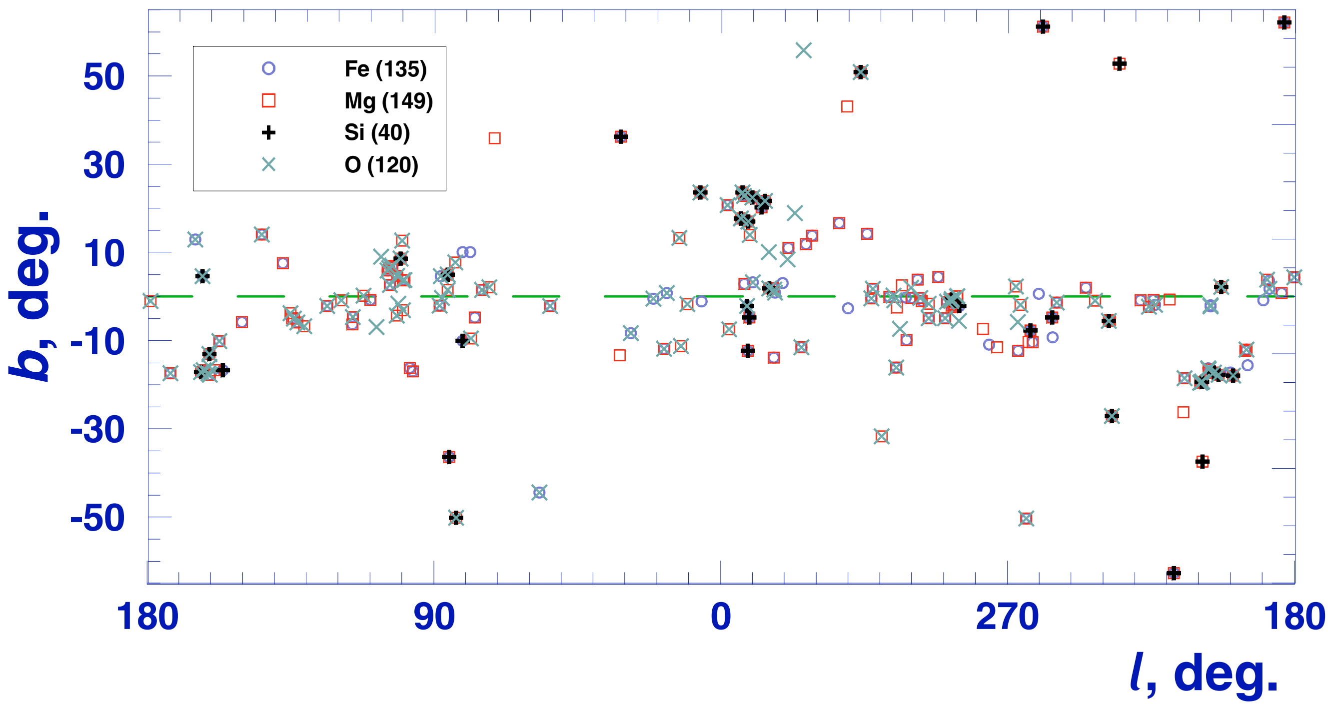

Fig. 1. Galactic distribution of stars studied in this paper. Sightlines with measured Fe, Mg, Si, and O are shown by different symbols. Number of stars considered is indicated in parentheses in the legend.

cannot be studied in such detail since the number of sightlines with measured carbon abundances does not exceed 20 (Sofia et al. 2004; J09), and at least in six directions they have been revised downward in comparison with earlier estimates (Sofia & Parvahti 2009). Our main goal is to establish what could be the real dust phase abundances and whether they could rule out ambiguity in modelling interstellar extinction, polarization, and spectral IR features.

2. Sample of stars and first analysis

2.1. Definitions

The abundance of an element in the interstellar medium is determined as a number of atoms relative to that of hydrogen, [X/H], where X (or N(X)) and H (or $N(\mathrm{H}) = N(\mathrm{HI}) + 2N(\mathrm{H_2})$) are the column densities of an element X and hydrogen in a given direction. The abundances by number are often expressed as the number of X atoms per 10^6 hydrogen nuclei (parts per million, ppm, hereafter).

Usually, the gas phase abundances of most elements $[\mathrm{X/H}]_\mathrm{g}$ are smaller than the corresponding "cosmic" (reference, solar) abundances. The depletion of an element X is defined by

$$D_\mathrm{X} = \left[\frac{\mathrm{X}}{\mathrm{H}}\right]_\mathrm{g} \Big/ \left[\frac{\mathrm{X}}{\mathrm{H}}\right]_\mathrm{cosmic}. \quad (1)$$

The logarithmic quantities

$$\delta_\mathrm{X} = \log D_\mathrm{X} = \log \left[\frac{\mathrm{X}}{\mathrm{H}}\right]_\mathrm{g} - \log \left[\frac{\mathrm{X}}{\mathrm{H}}\right]_\mathrm{cosmic} \quad (2)$$

are also used[1].

[1] The bracketed notation [X/H] and the units ppm are traditionally utilized when the dust phase abundances are studied (e.g., Greenberg 1978; Mathis 1996; Voshchinnikov 2004).

2.2. Data

We assume that interstellar atoms are in the dominant ionization stage for HI regions: OI, MgII, SiII, and FeII. The contribution of neutral atoms to the total column density of magnesium, silicon, and iron can be neglected (see, e.g., data of Savage & Bohlin 1979; and Gnaciński & Krogulec 2006). The presence of the HII regions on the line of sight may lead to some fraction of atoms in a stage of ionization above the preferred one. To exclude this effect, J09 deduces his fits for the sightlines with $N(\mathrm{H}) > 3 \times 10^{19}$ cm^{-2}, although later he finds small departure from a linear trend between the depletion factors F_* and the logarithm of the average density for sightlines with hydrogen column densities lower than 3×10^{19} cm^{-2}.

Our list of stars includes different targets with measured gas phase abundances of oxygen, magnesium, silicon, or iron. We transform all data into the unified (standard) system of oscillator strengths as given in Table 1 of J09. We also use the hydrogen column density from J09 when available[2]. The final sample contains 196 sightlines with 1σ errors (see Table A.1 in Appendix). Observational data are taken from J09, Cartledge et al. (2004, 2008), and Jensen et al. (2005) for oxygen (120 sightlines); J09, Jensen & Snow (2007b), Cartledge et al. (2006), Howk et al. (1999), and Gnaciński & Krogulec (2006) for magnesium (149); Jensen (2007), Gnaciński & Krogulec (2006), and J09 for silicon (40); and J09, Jensen & Snow (2007a), Snow et al. (2002), and Miller et al. (2007) for iron (135). For two sightlines (HD 93521 and HD 215733), where the data for separate velocity components are obtained, we take the total column densities. The galactic distribution of all 196 stars is plotted in Fig. 1. Overlapping symbols indicate that, for a given sightline measurements were made for more than one element. Figure 2 illustrates the distance distribution of stars in the projection on the galactic plane.

The abundances were supplemented with stellar distances D, colour excesses $E(B-V)$ and characteristics of the extinction

[2] N(H) for star CPD –59 2603 is taken from Jensen & Snow (2007a).

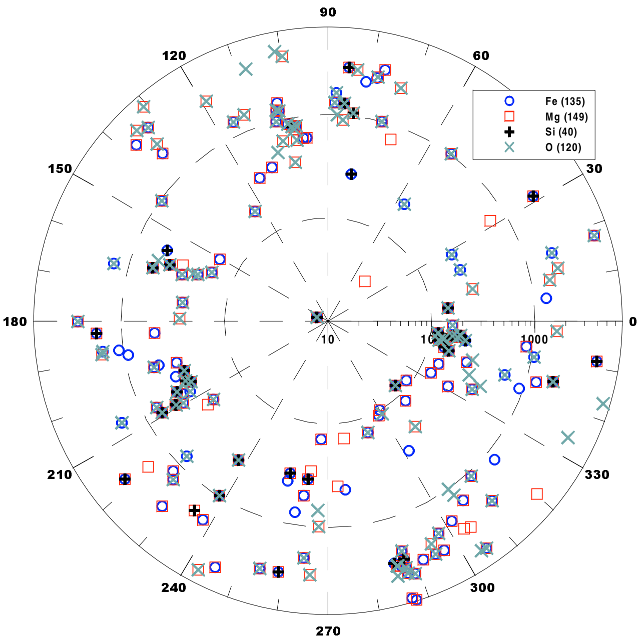

Fig. 2. Distance distribution of stars studied in this paper in polar representation. The Galactic centre is to the right. The distance from the Sun is plotted in logarithmic scale. Sightlines with measured Fe, Mg, Si, and O are shown with different symbols. Number of stars is indicated in parentheses.

curves: the ratio of total to selective extinction $R_V = A_V/E(B-V)$ and the parameters of UV extinction as suggested by Fitzpatrick & Massa (1990, 2007). Extinction data are collected from papers of Fitzpatrick & Massa (2007), Valencic et al. (2004), Wegner (2002, 2003), Patriarchi et al. (2003) and the papers with published abundances cited above.

We recalculated all colour excesses $E(B-V)$ published by J09 using normal colours of stars from Straižys (1992) and Landolt-Börnstein and spectral types from Bowen et al. (2008) and J09. This permits avoiding the difficulties with the negative values of $E(B-V)$ obtained by J09. Using the 2MASS K-magnitudes from the Simbad database, correction to the Johnson system given by Bowen et al. (2008) and normal colours $(V-K)_0$ from Straižys (1992) and Winkler (1997), we estimated colour excesses $E(V-K)$ for several stars. Next we found the ratio R_V with the aid of the relation $R_V = 1.1\,E(V-K)/E(B-V)$ (Voshchinnikov & Il'in 1987).

From the distance distribution of colour excesses plotted in Fig. 3, it follows that the major part of stars have $E(B-V) \lesssim 0.6$. This means that they are located behind diffuse atomic and molecular clouds or translucent interstellar clouds (see Table 1 in Snow & McCall 2006, for classification). In Fig. 3 we separate 16 stars located at high galactic latitudes $|b| > 30°$[3]. Previous considerations (e.g., Savage & Sembach 1996) indicate that the gas has smaller depletions in the lower halo in comparison with gas located in the galactic disk. The total hydrogen column density is smaller for stars observed at high galactic latitudes (Fig. 4). Figure 4 allows one to study the gas-to-dust ratio in the direction of stars from our sample. Ryter (1996) deduce the average gas-to-dust ratio

$$\frac{N(\mathrm{H})}{E(B-V)} = 6.56\times10^{21}\ \mathrm{atoms\,cm^{-2}\,mag^{-1}}\,, \quad (3)$$

[3] We include HD 38666 ($b = -27.1°$) where anomalous high gas phase abundances of Mg, Si, and Fe are observed in this list of stars.

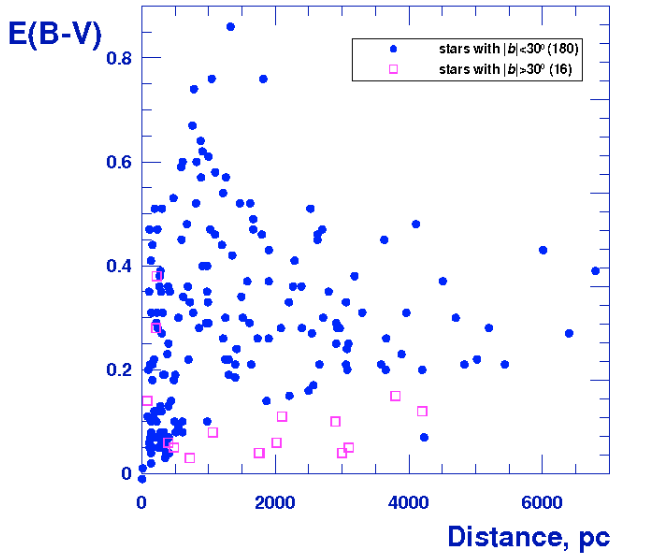

Fig. 3. Distance distribution of colour excess $E(B-V)$ for stars studied in this paper. Open squares show stars located at galactic latitudes $|b| > 30°$.

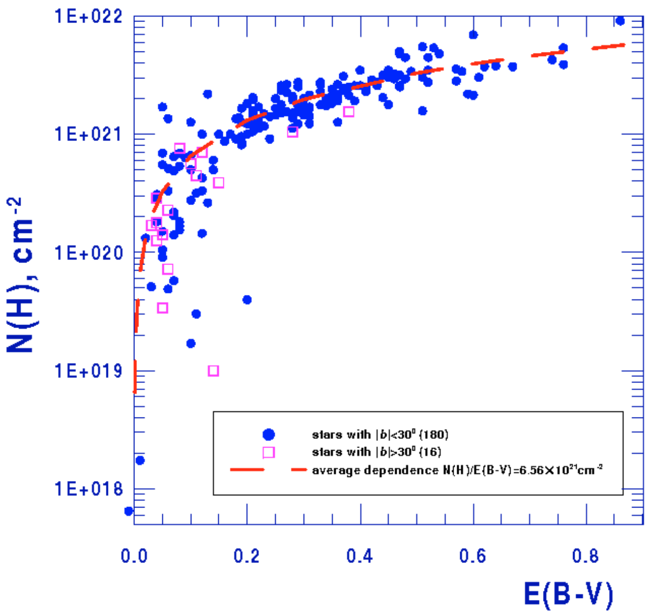

Fig. 4. Total hydrogen column density as function of the colour excess for stars studied in this paper. The dashed line shows the average dependence between N(H) and $E(B-V)$ deduced by Ryter (1996).

where the contribution of ionized hydrogen is neglected. From Fig. 4 it can be seen that the dependence of N(H) on $E(B-V)$ does not strongly deviate from the average dependence if $E(B-V) \gtrsim 0.2$. Near this value there is the border between diffuse and translucent interstellar clouds (Snow & McCall 2006). Observational errors are larger if the sightline crosses a diffuse cloud. For stars seen through the translucent clouds, the ratio $N(\mathrm{H})/E(B-V)$ lies within rather narrow limits from $\sim3\times10^{21}$ cm^{-2} mag^{-1} to $\sim1\times10^{22}$ cm^{-2} mag^{-1}. For almost all sightlines considered by us, the criterion of J09 ($N(\mathrm{H}) > 3\times10^{19}$ cm^{-2}) is satisfied. Two points in the lower left corner of Fig. 4 correspond to HD 34029 (Capella)[4] and HD 48915

[4] J09 gives the observed colour $B-V$ not $E(B-V)$ for Capella in Table 2.

(Sirius). The colour excesses for them are very small and uncertain, therefore we exclude these two stars from further analysis.

2.3. Reference abundances

We use, as a starting point, the solar abundances from Asplund et al. (2009) as cosmic abundances. These data are justified and are rather close to the modern solar system abundances recommended by Lodders et al. (2009). Taking $[\mathrm{O/H}]_\odot = 490$ ppm, $[\mathrm{Mg/H}]_\odot = 39.8$ ppm, $[\mathrm{Si/H}]_\odot = 32.4$ ppm, and $[\mathrm{Fe/H}]_\odot = 31.6$ ppm, and neglecting the errors in the reference abundances, we converted the gas phase abundances into the dust phase abundances

$$\left[\frac{\mathrm{X}}{\mathrm{H}}\right]_{\mathrm{d}} = \left[\frac{\mathrm{X}}{\mathrm{H}}\right]_{\mathrm{cosmic}} - \left[\frac{\mathrm{X}}{\mathrm{H}}\right]_{\mathrm{g}} = \left[\frac{\mathrm{X}}{\mathrm{H}}\right]_{\mathrm{cosmic}} (1 - D_{\mathrm{X}}) = \left[\frac{\mathrm{X}}{\mathrm{H}}\right]_{\mathrm{cosmic}} \left(1 - 10^{\delta_{\mathrm{X}}}\right). \quad (4)$$

2.4. Choice of external parameter and selection effects

Previous considerations reveal correlations between element depletion and an "external" parameter characterizing the gas density in the line of sight: $N(\mathrm{H})$, $\langle n(\mathrm{H})\rangle = N(\mathrm{H})/D$, $f(\mathrm{H}_2) = 2N(\mathrm{H}_2)/N(\mathrm{H})$ (see Jensen 2007; and J09 for detailed discussion). Clear trends toward increasing gas depletion (and correspondingly growth of dust phase abundances) are found for Mg, Si, and Fe with respect to $\langle n(\mathrm{H})\rangle$. Sometimes, variations in depletion with distance are also considered (Cartledge et al. 2006, 2008; Jensen 2007).

In deciding on the parameter connecting dust grains and abundances, we are restricted by reddening $E(B-V)$, extinction A_V and average reddening $E(B-V)/D$ or extinction A_V/D. In order to determine extinction, we must know the ratio R_V, which is not easily detected from observations (see discussion in Straižys 1992). It is also important that we only know total (summary) extinction or reddening and cannot separate individual clouds on the line of sight.

For further analysis, we choose the average reddening $E(B-V)/D$ as an external parameter because $E(B-V)$ and D are usually well known for different sightlines. Colour excess $E(B-V)$ (or reddening) characterizes the amount of dust on the line of sight and the properties of dust particles. It can be calculated as

$$E(B-V) = A_B - A_V \approx 1.086\,(\langle C_{\mathrm{ext},B}\rangle - \langle C_{\mathrm{ext},V}\rangle)\,N_{\mathrm{d}},$$

where N_{d} is the dust column density and $\langle C_{\mathrm{ext},B}\rangle$, $\langle C_{\mathrm{ext},V}\rangle$ are average extinction cross sections. Sightlines with low reddening may be the result of the absence of dust (low N_{d}-value) or similar cross sections in the B and V bands. The latter can be interpreted as the presence of large grains producing neutral extinction. Perhaps, such sightlines have higher hydrogen column density than average and appear as points above the curve at the left upper part of Fig. 4. However, one should keep in mind that the error of the colour excess is larger for lower values of $E(B-V)$[5].

Relative dust phase abundances of Mg, Si, and Fe are plotted in Fig. 5 in the form $[\mathrm{X/H}]_{\mathrm{d}}/[\mathrm{X/H}]_{\mathrm{cosmic}} = 1 - D_{\mathrm{X}}$ as a function of $E(B-V)/D$. Using Eq. (3), the average reddening can be translated into average gas density:

$$\langle n(\mathrm{H})\rangle\left[\mathrm{cm}^{-3}\right] \approx 2.13 \times E(B-V)/D[\mathrm{mag/kpc}].$$

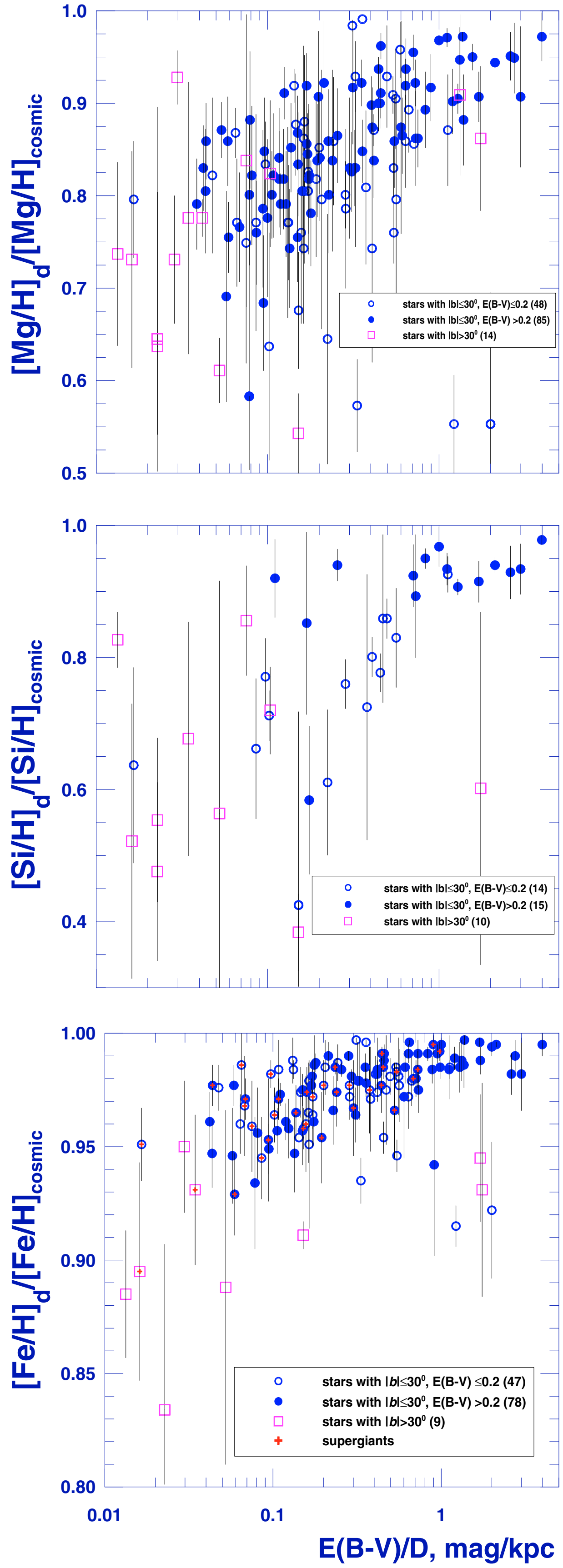

Fig. 5. Relative dust phase abundances of Mg, Si, and Fe with 1σ error bars in dependence on average reddening $E(B-V)/D$. Circles and squares show data for stars with $|b| \leq 30°$ and $|b| > 30°$, respectively. The number of stars is indicated in parentheses. Crosses in lower panel show data for supergiants.

[5] The polarimetric data obtained for stars with low reddening give the polarization efficiency close to average one $P/E(B-V) = 3\%$/mag (Berdyugin et al., in prep.).

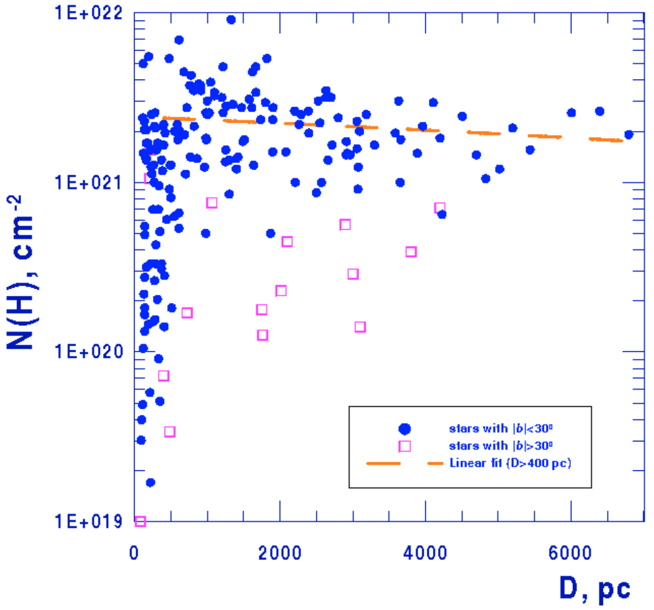

Fig. 6. Distance dependence of total hydrogen column density for stars studied in this paper. The dashed line is the fit for stars with $D > 400$ pc.

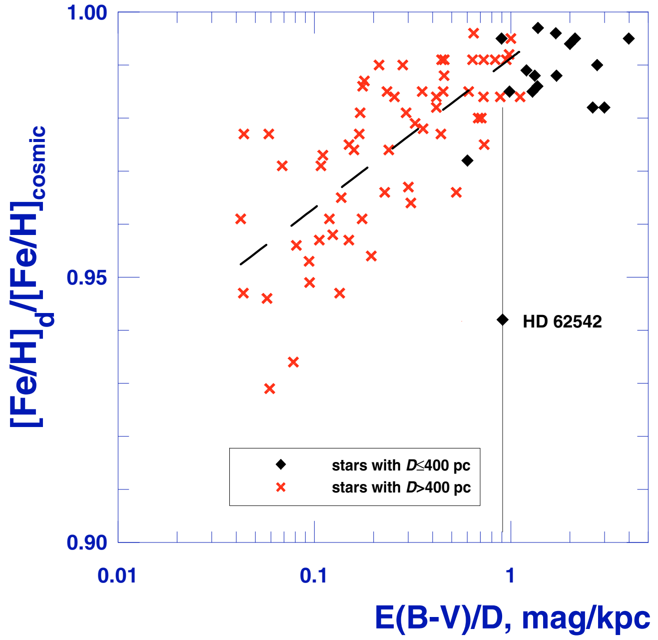

Fig. 7. Relative dust phase abundances of Fe as a function of average reddening $E(B-V)/D$ for stars with $|b| \leq 30°$ and $E(B-V) > 0.20$. Rhombuses and crosses show data for stars with $D \leq 400$ pc and $D > 400$ pc, respectively. The dashed line is the fit.

Stars in our sample are divided into two groups depending on their position in the Galaxy: stars at high galactic latitudes ($|b| > 30°$) and stars located near the disk ($|b| \leq 30°$), which in turn are separated as sightlines passing through diffuse ($E(B-V) \leq 0.20$) and translucent ($E(B-V) > 0.20$) clouds. It can be seen that the abundances for high-latitude and disk sightlines are quite different. For high-latitude stars, the element fraction in dust is lower and does not depend on the average reddening. This is well established and was interpreted in the homework of the Spitzer (1985) model of the different grain composition in the warm and cold phases of the ISM.

For disk stars, independent of reddening, there is a smooth decrease in the dust phase abundances of Mg, Si, and Fe when $E(B-V)/D$ grows smaller. This is expected in the context of previous findings (Jensen 2007; J09). The reason for such behaviour may be some physical processes lower cosmic abundances outside the solar environment or observational selection. Selection effects can appear for distant stars as they may be more luminous and produce more UV flux that can modify gas abundances. To check this we mark out in Fig. 5 (lower panel) 19 supergiants. It is evident that the directions to supergiants are not peculiar and fall well into the general pattern of disk and high-latitude stars. Therefore, differences in the types of material probed along more and less luminous stars seem cannot cause the trends observed in Fig. 5.

The true reason of decreasing dust phase abundances (and correspondingly increasing gas phase abundances) for smaller $E(B-V)/D$ and $\langle n(\mathrm{H})\rangle$ is evident from Fig. 6 (see also Fig. 3). *A systematic tendency exists for a decrease in the observed hydrogen column density and colour excess for distant stars.* In our sample (178 sightlines with $|b| \leq 30°$), the decrease is observed for stars with $D \gtrsim 400$ pc with the gas-to-dust ratio remaining almost constant for clouds located at different distances. As a result of lower hydrogen column density for distant stars, we obtain a clear trend for abundances as a function of any parameter related to the gas or dust density or distance. Figure 7 illustrates this observational selection effect. It shows the ratio $[\mathrm{Fe/H}]_{\mathrm{d}}/[\mathrm{Fe/H}]_{\mathrm{cosmic}}$ in dependence on $E(B-V)/D$ for stars observed through translucent interstellar clouds. Apparently, many previous correlations of interstellar abundances reflect a decrease in $N(\mathrm{H})$ and $E(B-V)$ with increasing D. It looks like we observe less and less dense clouds when the distance grows. Evidently, this problem requires further investigation, especially observations of high-density longer sightlines.

3. Results and discussion

3.1. Mean values and deviations

Mean element abundances locked up in dust are given in Table 2. The data are presented for all sightlines and separately for high-latitude and disk stars having low and high reddening, respectively. Distinctions between the various groups are noticed. For all three elements the following inequality is valid:

$$\langle[\mathrm{X/H}]_{\mathrm{d}}\rangle_{|b|>30°} < \langle[\mathrm{X/H}]_{\mathrm{d}}\rangle_{|b|<30°,\,E(B-V)\leq 0.2} < \langle[\mathrm{X/H}]_{\mathrm{d}}\rangle_{|b|<30°,\,E(B-V)>0.2}\,.$$

As follows from Fig. 5, halo ($z \gtrsim 150$ pc) and disk stars can be easily distinguished by the average reddening. For halo stars we have $E(B-V)/D \lesssim 0.05$ mag/kpc. Exceptions are three short high-latitude sightlines for HD 116658 ($b = +50.8°$, $D = 80$ pc), HD 203532 ($b = -31.7°$, $D = 211$ pc), and HD 210121 ($b = -44.4°$, $D = 223$ pc). They cross relatively dense clouds (see also Fig. 3) and have abundances similar to those of halo stars. The upper right corner of Fig. 5 is mainly filled by reddened nearby stars. A dividing line between stars with distances greater or less than 400 pc passes near the value $E(B-V)/D \approx 1$ mag/kpc (Fig. 7). Because the data for stars with $D \gtrsim 400$ pc seems to be "infected" with observational bias, we also calculated the mean abundances for nearby stars. A noticeable growth of abundances occurs for reddened disk stars. The results are shown in Table 2 in italics.

There are several sightlines where the dust phase abundances of Mg and Fe are significantly lower than the general trends

Table 2. Mean value of element abundance in dust phase in ppm with 1σ error.

	$\langle[\mathrm{Mg/H}]_\mathrm{d}\rangle$	$\dfrac{\langle[\mathrm{Mg/H}]_\mathrm{d}\rangle}{[\mathrm{Mg/H}]_\mathrm{cosmic}}$	$\langle[\mathrm{Si/H}]_\mathrm{d}\rangle$	$\dfrac{\langle[\mathrm{Si/H}]_\mathrm{d}\rangle}{[\mathrm{Si/H}]_\mathrm{cosmic}}$	$\langle[\mathrm{Fe/H}]_\mathrm{d}\rangle$	$\dfrac{\langle[\mathrm{Fe/H}]_\mathrm{d}\rangle}{[\mathrm{Fe/H}]_\mathrm{cosmic}}$
all sightlines	33.13 ± 2.35	0.832 ± 0.059 (147)*	25.01 ± 2.91	0.772 ± 0.090 (39)	30.64 ± 0.41	0.970 ± 0.013 (134)
stars with $\lvert b\rvert \le 30°$						
$E(B-V) \le 0.20$	32.31 ± 2.60	0.812 ± 0.065 (48)	23.97 ± 3.03	0.740 ± 0.093 (14)	30.65 ± 0.40	0.970 ± 0.013 (47)
$E(B-V) > 0.20$	34.11 ± 1.96	0.857 ± 0.049 (85)	29.30 ± 1.48	0.904 ± 0.046 (15)	30.86 ± 0.31	0.977 ± 0.010 (78)
	36.90 ± 1.44	*0.927 ± 0.036 (14)*	*30.25 ± 0.76*	*0.934 ± 0.023 (6)*	*31.16 ± 0.31*	*0.986 ± 0.010 (17)*
stars with $\lvert b\rvert > 30°$	29.98 ± 3.92	0.753 ± 0.099 (14)	20.03 ± 4.90	0.618 ± 0.151 (10)	28.68 ± 1.30	0.908 ± 0.041 (9)

Notes. (*) Number of sightlines. Results for stars with $D \le 400$ pc and $|b| \le 30°$, $E(B-V) > 0.20$ are given in italics.

clearly seen in Fig. 5. The major part of "peculiar" sightlines is related to stars with $E(B-V) \le 0.2$. Only two objects (HD 62542 and HD 99890) are observed through translucent clouds, but the observational errors are quite large in these cases. Note also that the shape of the UV extinction curve in the direction of HD 62542 is very peculiar (Voshchinnikov & Das 2008). It should be remembered that almost all stars with anomalous low dust phase abundances are located in Carina-Centaurus at the galactic longitudes $l \approx 290°-330°$.

We compared our results with data presented in Table 4 of J09, which gives element depletion parameters corresponding to the cases of "full depletion" ($F_* = 1$) and "no depletion" ($F_* = 0$). We transformed these parameters into our reference system and find the relative dust phase abundances of Mg, Si, and Fe. They are equal to $[\mathrm{Mg/H}]_\mathrm{d}/[\mathrm{Mg/H}]_\mathrm{cosmic} = 0.94$ and 0.44, $[\mathrm{Si/H}]_\mathrm{d}/[\mathrm{Si/H}]_\mathrm{cosmic} = 0.94$ and 0.25, and $[\mathrm{Fe/H}]_\mathrm{d}/[\mathrm{Fe/H}]_\mathrm{cosmic} = 0.99$ and 0.88 for the cases $F_* = 1$ and $F_* = 0$, respectively. The data for the "full depletion" case are well within our results (see Table 2 and Fig. 5). For another case ("no depletion"), the abundances of J09 seem to be too low even for high-latitude stars. This may be a result of observational selection and smaller number of sightlines in comparison with our sample.

3.2. Correlations

Using our data it is possible to plot the dust phase abundance of one element against that of another element. Such diagrams clearly show the existence of strong correlations between the abundances of Mg, Si, and Fe for low reddened and distant stars (see, e.g., Cartledge et al. 2006; Miller et al. 2007). However, these correlations trace the behaviour of the hydrogen column density discussed in Sect. 2.4.

To exclude the effect of N_H we plot the ratio of the dust phase abundances of Fe to Mg in dependence on the average reddening. The result is shown in Fig. 8 for 104 sightlines with the linear regression fit for 56 disk sightlines with $E(B-V) > 0.20$ (HD 99890 was excluded) as derived by a χ^2 minimization that takes error bars into account. The Pearson correlation coefficient for these sightlines is $r_\mathrm{corr} = -0.73$. As follows from Fig. 8, the amount of iron grows slightly in comparison with the amount of magnesium when the average reddening decreases. Twelve stars have distances $D < 400$ pc. They are located in the bottom right part of Fig. 8 and have an almost constant ratio Fe/Mg ≈ 0.84.

A similar behaviour can be observed if we compare dust phase abundances of Mg or Fe and Si. However, in this case the number of sightlines is three times less, because it is dictated by the measurements of silicon (see Figs. 1 and 2). For almost all sightlines with measured Si we have measurements of Mg and Fe. Therefore, one can consider the composition of grains.

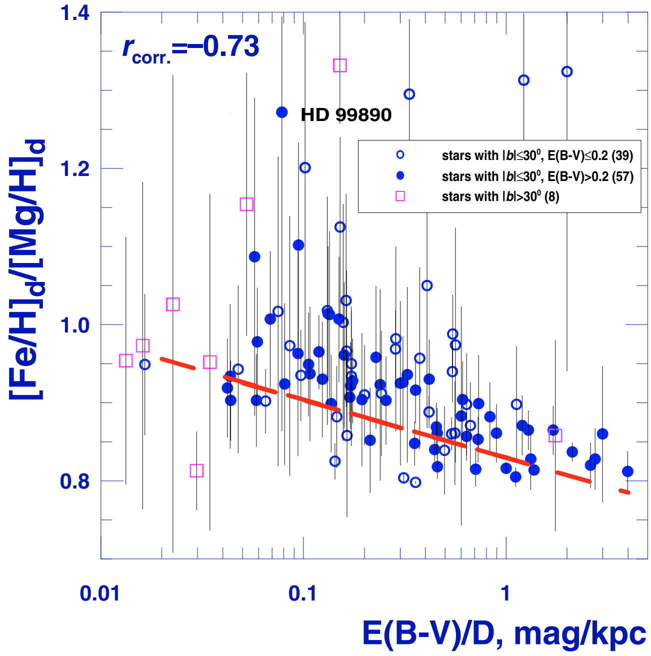

Fig. 8. Ratio of dust phase abundances of Fe and Mg in dependence on average reddening $E(B-V)/D$. Open and filled circles show data for disk stars with $E(B-V) \le 0.20$ and $E(B-V) > 0.20$, respectively. Squares correspond to sightlines with $|b| > 30°$. The bold dashed line is the linear regression fit for stars with $E(B-V) > 0.20$: $[\mathrm{Fe/H}]_\mathrm{d}/[\mathrm{Mg/H}]_\mathrm{d} = (-0.074 \pm 0.010)\log[E(B-V)/D] + (0.830 \pm 0.003)$.

3.3. Olivines, pyroxenes, and...?

All elements considered by us are constituents of cosmic silicate grains showing a pronounced 9.7 μm feature observed in spectra of a wide variety of objects (see Henning 2009, for a recent review). The origin of this feature is related to the stretching of the Si-O bond in amorphous silicates with olivine ($\mathrm{Mg}_{2x}\mathrm{Fe}_{2-2x}\mathrm{SiO}_4$) or pyroxene ($\mathrm{Mg}_y\mathrm{Fe}_{1-y}\mathrm{SiO}_3$) stoichiometry, where $0 \le x, y \le 1$. If we assume that Mg, Si, and Fe are incorporated only into Mg-Fe silicates, the ratio of (Fe+Mg)/Si in the dust phase must be in the range from 1 to 2, while the ratios Mg/Si and Fe/Si may vary from 0 to 2.

Figure 9 shows the ratios as a function of average reddening for 31 sightlines where joint measurements of abundances of Mg, Si, and Fe are available. As follows from Fig. 9 (upper panel), the ratio (Fe + Mg)/Si > 2 for all stars. This ratio may exceed 3 for low-reddened and high-latitude stars. For high reddened stars (excluding CPD −59 2603), the ratio (Fe + Mg)/Si lies in a narrow range from 2.15 to 2.35. The average value for 13 sightlines is $\langle(\mathrm{Fe+Mg})/\mathrm{Si}\rangle = 2.25 \pm 0.14$.

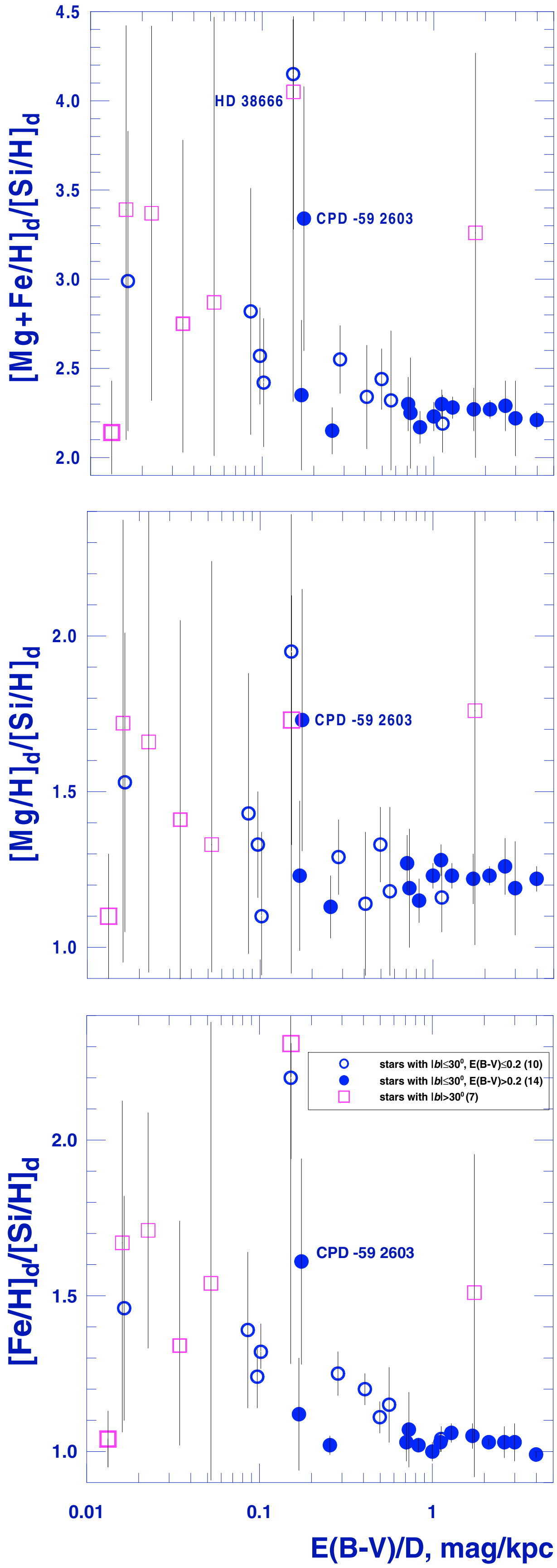

Fig. 9. Ratio of dust phase abundances of (Fe+Mg)/Si, Mg/Si, and Fe/Si with 1σ error bars in dependence on average reddening for 31 sightlines with joint measurements of three elements. Open and filled circles show data for sightlines with diffuse and translucent interstellar clouds, respectively. Squares correspond to high-latitude stars.

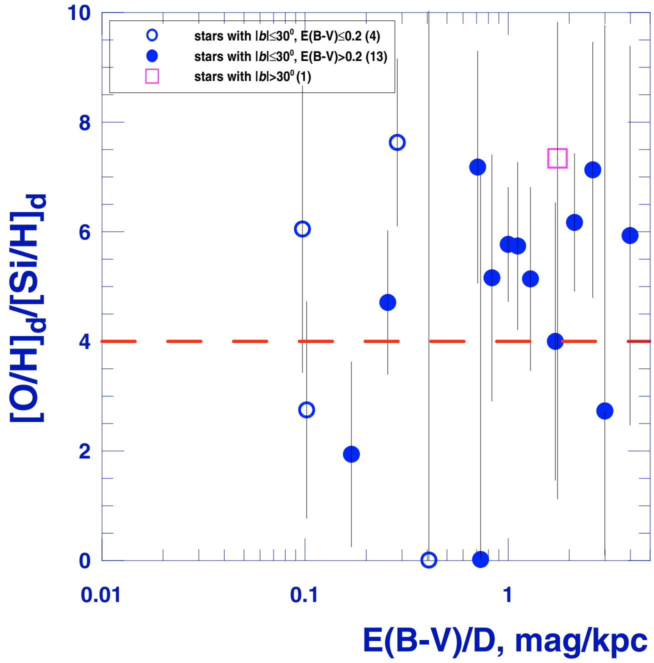

Fig. 10. Ratio of dust phase abundances of O and Si with 1σ error bars reduced twice in dependence on average reddening $E(B-V)/D$. Open and filled circles show data for disk stars seen through diffuse and translucent interstellar clouds, respectively. Squares correspond to sightlines with $|b| > 30°$.

The middle and low panels of Fig. 9 demonstrate that magnesium and iron are incorporated into dust particles in unequal parts for high and low reddened stars and high-latitude stars. For disk stars with $E(B-V) > 0.20$, the composition of grains averaged over 13 targets is $Mg_{1.22}Fe_{1.04}SiO_{z1}$. This composition cannot be reproduced by the mixture of olivine and pyroxene silicates alone with any value of x and y. It indicates that some amount of magnesium or iron (or both) should be embedded in another population of dust grains, probably, metal oxides.

When we consider high-latitude stars, averaging over 6 targets (excluding HD 38666) gives the "grain composition" $Mg_{1.50}Fe_{1.47}SiO_{z2}$[6]; i.e., the ratio Fe/Mg is greater for high-latitude stars than for disk stars. This suggests that the destruction of Mg-rich grains in the warm medium is more effective than of Fe-rich grains.

3.4. ... + Problematic O

The sample of stars discussed in Sect. 3.3 includes 20 sightlines where the abundances of OI have also been measured. Thus, we can compare abundances of four elements. We plot oxygen abundances in Figs. 10 and 11. The error bars are twice reduced in comparison with those observed in these figures. Unfortunately, the uncertainties in determining of the gas phase oxygen abundances are too large to allow any definitive answer about the trends in oxygen depletion.

Figure 9 clearly shows the excess of both iron and magnesium over silicon, so if we assume that all Si atoms are incorporated into olivine, the O to Si ratio must be equal to or exceed 4. This ratio is plotted in Fig. 10 for 18 sightlines[7]. It is interesting

[6] The values of $z1$, $z2$ are not the same and must lie between 3 and 4 for a mixture of pyroxene and olivine grains.

[7] Two sightlines (towards HD 38666 and HD 141637) with $[O/H]_d < 0$ are omitted.

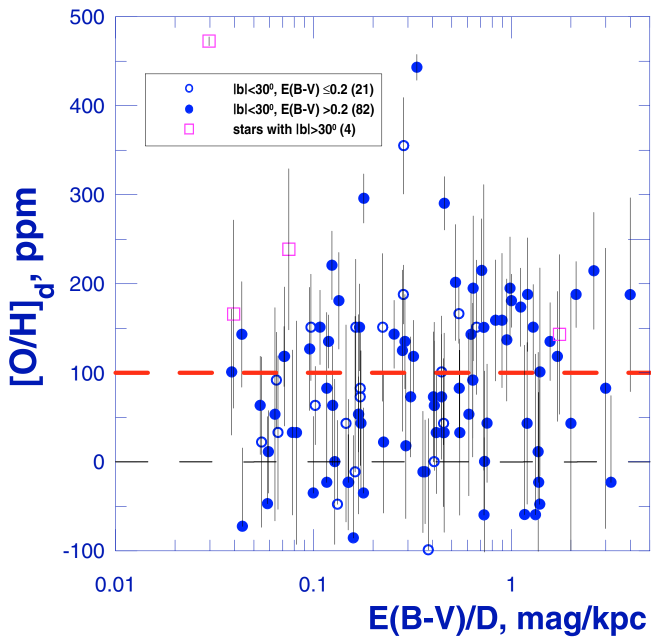

Fig. 11. Dust phase abundances of O in ppm with 1σ error bars reduced in twice in dependence on average reddening $E(B-V)/D$. Open and filled circles show data for disk stars seen through diffuse and translucent interstellar clouds, respectively. Squares correspond to sightlines with $|b| > 30°$.

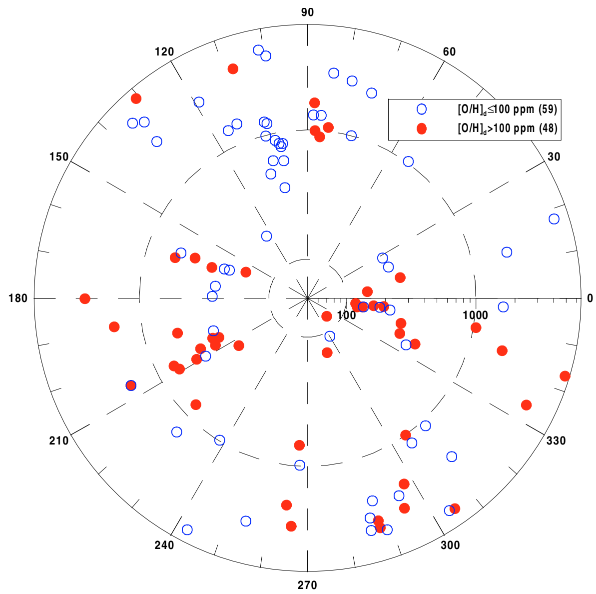

Fig. 12. Distance distribution of stars with $[O/H]_d \leq 100$ ppm (open circles) and $[O/H]_d > 100$ ppm (filled circles) in polar representation. The Galactic centre is to the right. The distance from the Sun is plotted in logarithmic scale. Number of stars is indicated in parentheses.

that, for 10 of 13 stars observed through translucent clouds, the ratio $[O/H]_d/[Si/H]_d \geq 4$. This means that we have enough O for silicate particles and, perhaps, some additional oxygen for producing oxides and ices. However, this effect may be related to the regional variations in oxygen abundances as all these stars are located in the bottom part of Fig. 2, i.e., at the galactic longitudes $l \approx 180°-360°$.

In Fig. 11 we plot the oxygen dust phase abundances for our sample of stars. These abundances were found as the difference between solar oxygen abundance (490 ppm) and observed gas phase abundances. The data are shown for 107 sightlines (12 sightlines where $[O/H]_d < -150$ ppm were omitted). The absence of trends and correlations as seen for Mg, Si, or Fe (Fig. 5) is obvious. For many directions the dust phase abundances of O are negative and primarily related to large observational errors. We can make a tentative inference about the deficit (not excess!) of oxygen in the dust phase opposite to the conclusion of J09. In the case of using proto-Sun oxygen abundance ($[O/H]_\odot$ = 575 ppm from Lodders 2003), things will not get much better, so it seems too early to search for the "missing oxygen" in the dust phase (Whittet 2010).

We divided the stars into two groups: with $[O/H]_d >$ 100 ppm and $[O/H]_d \leq 100$ ppm. This border value is calculated as the product 4×25, assuming the mean value for Si from Table 2 and assuming that all Si atoms are tied up into olivine-type silicates[8]. Such a division reveals an interesting galactic distribution of the "O-rich" and "O-poor" sightlines shown in Fig. 12. It can be seen that the open and filled circles are not well mixed. There are areas on the sky where the symbols of one type concentrate. Particularly striking is the zone between $l \approx 70°$ and $l \approx 140°$ (Cygnus, Cassiopea, Perseus) where 23 of 59 stars with reduced O abundance in dust are located. Perhaps, this behaviour does not merely reflect the observational errors and indicate the existence of an another non-solar cosmic standard with enhanced metal abundances in this area. This hypothesis is partially supported by a higher fraction of metal-rich Cepheids found at these galactic longitudes (see Fig. 5 in Pedicelli et al. 2009).

3.5. Correlation with extinction and regional variations

The elements of C, O, together with Mg, Si, and Fe as studied here contribute to most of the mass of the interstellar dust. Therefore, it is interesting to study a dependence of dust phase abundances on the ratio R_V. The ratio of total to selective extinction R_V characterizes the visual extinction produced by dust particles with radii $r \gtrsim 0.05\,\mu$m (e.g., Voshchinnikov 2004). The search for a correlation between depletions $D_{\rm O,\,Mg,\,Fe}$ and R_V has been attempted by Jensen (2007), who finds no correlation for Mg and Fe and a slight trend to increasing OI depletion with increasing R_V.

In our sample there are 164 stars with known or calculated values of R_V. We found no significant correlation of dust phase abundances with R_V either for the total sample or for the disk stars with low and high reddening. Very probably, the absence of correlation is a consequence of the mixture of short and long sightlines in different galactic directions.

We investigated the regional variations of depletions and R_V. The difference in iron depletion was found by Savage & Bohlin (1979) for sightlines in Cygnus and Scorpius-Ophiuchus, while Patriarchi et al. (2003) and Wegner (2003) discovered the difference in R_V between stars in Cygnus and Carina and stars belonging to separate associations, respectively.

To exclude the distance effects discussed in Sect. 2.4 we only considered reddened stars with $D \lesssim 450$ pc. From this subsample of 25 sightlines, we separated two groups of stars more or less closely located on the sky (see also Figs. 1 and 2 and Table A.1): four stars in Perseus ($b = -13° \div -17°$, l = $160°-173°$, $D \approx 220-420$ pc, N(H) = $(1.26-1.95) \times 10^{21}$ cm^{-2}, $E(B-V)$ = 0.27–0.36) and seven stars in Scorpius-Ophiuchus

[8] Models of dust evolution predict a dust phase abundance of oxygen at a level of about 130 ppm at the modern time (see, e.g., Fig. 16 in Zhukovska et al. 2008).

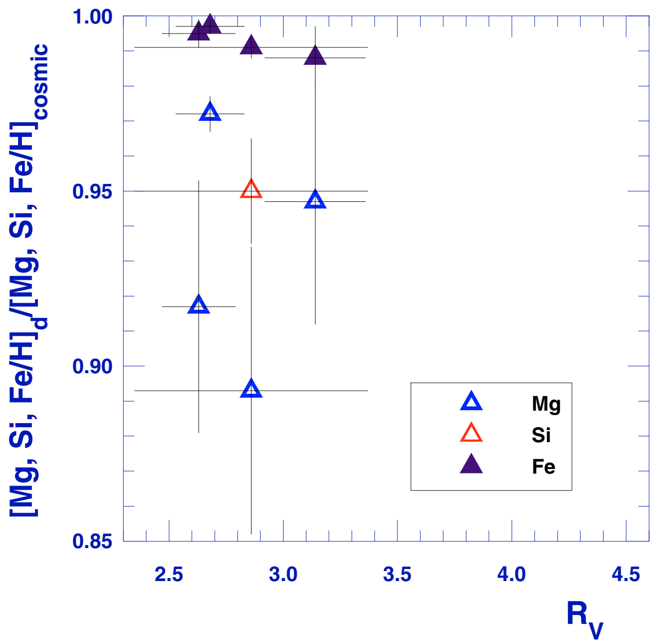

Fig. 13. Relative dust phase abundances of Mg, Si, and Fe with 1σ error bars in dependence on R_V for stars located in Perseus. The data correspond to the stars (*from left to right*): HD 24398, HD 27778, HD 24912, and HD 23180. The values of R_V were taken from Fitzpatrick & Massa (2007) for HD 23180 and HD 27778, Wegner (2003) for HD 24398 and Valencic et al. (2004) for HD 24912.

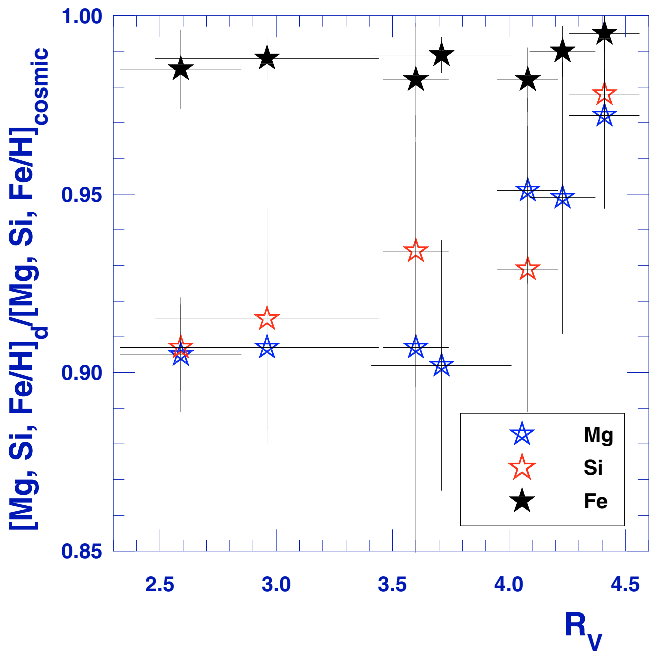

Fig. 14. The same as in Fig. 13 but now for stars located in Scorpius-Ophiuchus. The data correspond to the stars (*from left to right*): HD 144217, HD 143275, HD 147165, HD 144470, HD 147888, HD 148184, and HD 147933. The values of R_V were taken from Fitzpatrick & Massa (2007) for HD 144470, HD 147165, HD 147888, and HD 147933 and Lewis et al. (2009) for HD 143275, HD 144217, and HD 148184.

(b = 17°–23°, l = 350°–358°, $D \approx$ 120–200 pc, N(H) = (1.38–5.50) $\times 10^{21}$ cm^{-2}, $E(B-V)$ = 0.21–0.51). Three of them (HD 147165, HD 147888, and HD 147933) belong to the Eastern Group of the ρ Oph cloud, while four other stars belong to the Northern Group (Snow et al. 2008). The measured abundances of Mg, Si, and Fe are compared with R_V in Figs. 13 and 14. For stars in Perseus, the value of R_V is lower, on average, than the mean galactic value $R_V = 3.1$. In this case the correlation between dust phase abundances and R_V is absent (Fig. 13). For stars in Scorpius-Ophiuchus, R_V varies from ~2.6 to ~4.4. Figure 14 shows a clear growth of silicon and magnesium abundances in dust with increasing R_V[9]. The Pearson correlation coefficients are $r_{\rm corr} = 0.81$ for Mg and $r_{\rm corr} = 0.86$ for Si. This is the first evidence of a correlation of dust phase abundances with the ratio R_V. Although the correlation coefficients are relatively large, one should keep in mind the small number of sightlines. Since R_V is considered as a measure of grain size (Whittet 2003), we conclude that *accretion of Si and Mg atoms on large grains takes place.* Note also that obviously the abundance of iron is independent of the value of R_V.

For three stars in Perseus and four stars in Scorpius-Ophiuchus the extinction curve in the far-UV is also known. Fitzpatrick & Massa (2007) fit the observed far-UV extinction using two parameters c_4 and c_5, entering into a formula for the entire UV extinction. These parameters characterize the departure, in the far-UV, from the extrapolated bump-plus-linear components and indicate the strength of the far-UV curvature (c_4) and the wavenumber in μm^{-1} from which the far-UV extinction starts to grow (c_5). We interpret parameter c_4 as a measure of the relative amount of small grains (the slope of the size distribution function, e.g., the power index q in the power-law size distribution $n(r) \propto r^{-q}$) and parameter c_5 as a measure of the minimum particle size $r_{\rm min}$ in the dust ensemble.

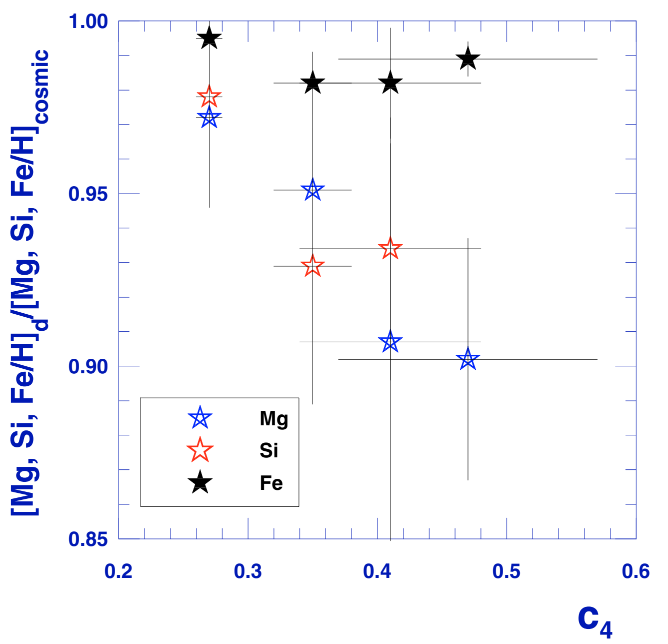

Fig. 15. Relative dust phase abundances of Mg, Si, and Fe with 1σ error bars as a function of UV extinction curve parameter c_4 (the strength of the far-UV curvature) for stars located in Scorpius-Ophiuchus. The data correspond to the stars (*from left to right*): HD 147933, HD 147888, HD 147165, and HD 144470.

Unfortunately, the limited data for Perseus do not allow a careful analysis. For stars located in Scorpius-Ophiuchus the normalized far-UV extinction is lower than the average Galactic extinction curve, which points to a deficit of the particles of small sizes. Figures 15 and 16 show the anticorrelation of the dust phase

[9] A similar trend is seen if we replace R_V by N(H).

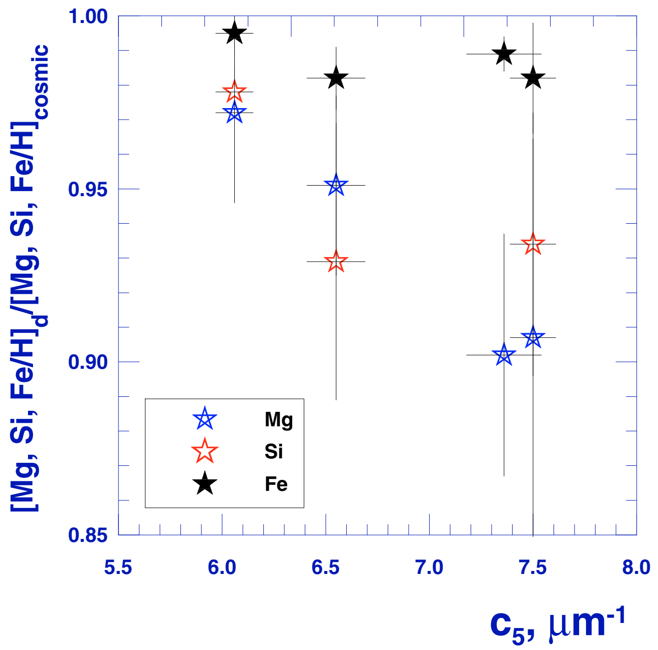

Fig. 16. Relative dust phase abundances of Mg, Si, and Fe with 1σ error bars as a function of UV extinction curve parameter c_5 (wavenumber from which the far-UV extinction starts to grow) for stars located in Scorpius-Ophiuchus. The data correspond to the stars (*from left to right*): HD 147933, HD 147888, HD 144470, and HD 147165.

abundances of Mg and Si with parameters c_4 and c_5 (the correlation coefficients are from $r_{\rm corr} = -0.70$ to $r_{\rm corr} = -0.99$). The shift from right to left in these figures indicates the decrease in q and increase in $r_{\rm min}$ (see, e.g., Voshchinnikov & Il'in 1993; and Fig. 24 in Voshchinnikov 2004). This flattening of the size distribution function and growth of minimum grain size is accompanied by the increase in the dust phase fraction of Mg and Si; i.e., *smaller grains are built up due to accretion of atoms from the gas*. Apparently, this occurs in clouds with the hydrogen column density $N(\rm H) \gtrsim 2 \times 10^{21}$ cm^{-2} resulting in after the propagation of a low-velocity shock (Meyers et al. 1985). Our arguments in favour of grain growth by accretion are supported by the results of a detailed interpretation of extinction for two stars made by Das et al. (2010). They find that for silicate grains $r_{\rm min} = 0.07\,\mu$m, $q = 2.0$ for HD 147933 and $r_{\rm min} = 0.04\,\mu$m, $q = 2.2$ for HD 147165.

The uniform variations in abundances of Mg and Si with R_V, N(H), c_4, and c_5 cannot be explained by grain coagulation because in this case the gas and dust phase abundances of elements are kept constant.

4. Conclusions

We investigated the differences in interstellar dust phase abundances of Mg, Si, and Fe entering into the composition of silicate and oxide grains. The distinctions in abundances can be separated into the following groups.

1. A sharp distinction in abundances is observed for sightlines located at low ($|b| < 30°$) and high ($|b| > 30°$) galactic latitudes. This is well known from previous studies. For high-latitude stars the ratios Mg/Si and Fe/Si in dust are close to 1.5. For disk stars these ratios are reduced to ~1.2 and ~1.05 for Mg and Fe, respectively. The derived numbers indicate that the dust grains cannot be just a mixture of only olivine and pyroxene silicates. Some amount of magnesium or iron (or both) should be embedded into another population, probably oxides.
2. We reveal a clear distinction in abundances for nearby ($D \lesssim 400$ pc) and distant ($D \gtrsim 400$ pc) stars: decrease in dust phase abundances and correspondingly increase in gas phase abundances with growth in D. We attribute this distinction to an observational selection effect: a systematic trend toward lower observed hydrogen column density for distant stars. As a result, we obtain a clear trend for abundances as a function of any parameter related to the gas or dust density or distance.
3. The less pronounced difference in abundances is found for disk stars with low ($E(B-V) \lesssim 0.2$) and high ($E(B-V) \gtrsim 0.2$) reddenings. This reflects the distinction between sightlines passing through diffuse and translucent interstellar clouds.
4. Regional variations of abundances of Mg, Si, and Fe are not evident. However, for Scorpius-Ophiuchus, we established an uniform increase of dust phase abundances in Mg and Si with an increase in the ratio of total to selective extinction R_V and an decrease in the strength of the far-UV extinction. Thus it is valid to say that there is a growth in Mg-Si grains due to accretion.

The uncertainties in determing of the oxygen abundances are large and do not allow one to make definitive conclusions about the oxygen depletion. We can only indicate a possible regional peculiarity in the zone between $l \approx 70°$ and $l \approx 140°$ (Cygnus, Cassiopea, Perseus) where many stars with reduced O abundance in dust are located.

Acknowledgements. We thank Adam Jensen for sending data for silicon, Andrei Berdyugin for sending the polarimetric results, and Vladimir Il'in, Jacek Krełowski, Piotr Gnaciński, Ralf Siebenmorgen, Svitlana Zhukovska, and Ted Snow for stimulating discussions. Special thanks go to the anonymous referee for helpful comments and suggestions. The work was partly supported by grants RFBR 07-02-00831, RFBR 10-02-00593a, NTP 2.1.1/665 and NSh 1318.2008.2.

References

Asplund, M., Grevesse, N., & Sauval, A. J. 2005, in Cosmic Abundances as Records of Stellar Evolution and Nucleosynthesis, ed. Th. G. Barbes, & F. N. Bash, ASP Conf. Ser., 336, 25
Asplund, M., Grevesse, N., Sauval, A. J., & Scott, P. 2009, ARA&A, 47, 481
Bowen, D. L., Jenkins, E. B., Tripp, T. M., et al. 2008, ApJS, 176, 59
Cartledge, S. I. B., Lauroesch, J. T., Meyer, D. M., & Sofia, U. J. 2004, ApJ, 613, 1037
Cartledge, S. I. B., Lauroesch, J. T., Meyer, D. M., & Sofia, U. J. 2006, ApJ, 641, 327
Cartledge, S. I. B., Lauroesch, J. T., Meyer, D. M., Sofia, U. J., & Clayton, G. C. 2008, ApJ, 687, 1043
Das, H. K., Voshchinnikov N. V., & Il'in, V. B. 2010, MNRAS, 404, 265
Field, G. B. 1974, ApJ, 187, 453
Fitzpatrick, E. L., & Massa, D. L. 1990, ApJS, 72, 163
Fitzpatrick, E. L., & Massa, D. L. 2007, ApJ, 663, 320
Gnaciński, P., & Krogulec, M. 2006, AcAstr, 56, 373
Greenberg, J. M. 1978, in Cosmic Dust, ed. by J. A. M. McDonnel, 187
Harris, A. W., Gry, C., & Bromage, G. E. 1984, ApJ, 284, 157
Henning, Th. 2009, in Interstellar Dust from Astronomical Observations to Fundamental Studies, ed. F. Boulanger et al., ESA Publ. Ser., 35, 103
Howk, J. C., Savage, B. D., & Fabian, D. 1999, ApJ, 525, 253
Jenkins, E. B., Savage, B. D., & Spitzer, L. 1986, ApJ, 301, 355
Jenkins, E. B. 2004, in Origin and Evolution of the Elements, ed. A. Mc William, & W. Rauch (Cambridge: Cambridge Univ. Press), 336
Jenkins, E. B. 2009, ApJ, 700, 1299 (J09)
Jensen, A. G. 2007, Ph.D. Thesis, University of Colorado

Jensen, A. G., & Snow, T. P. 2007a, ApJ, 669, 378
Jensen, A. G., & Snow, T. P. 2007b, ApJ, 669, 401
Jensen, A. G., Rachford, B. L., & Snow, T. P. 2005, ApJ, 619, 891
Jones, A. P. 2000, J. Geophys. Res., 105, 10257
Lewis, N. K., Cook, T. A., Wilton, K. P., et al. 2009, ApJ, 706, 306
Li, A., & Greenberg, J. M. 1997, A&A, 323, 566
Lodders, K. 2003, ApJ, 591, 1220
Lodders, K., Palme, H., & Gail, H.-P. 2009, in Landolt-Börnstein, New Series, Astronomy & Astrophysics (Springer), in press [arXiv:0901.1149]
Mathis, J. S. 1996, ApJ, 472, 643
Meyers, K. A., Snow, T. P., Federman, S. R., & Breger, M. 1985, ApJ, 288, 148
Miller, A., Lauroesch, J. T., Sofia, U. J., Cartledge S. I. B., & Meyer, D. M. 2007, ApJ, 659, 441
Patriarchi, P., Morbidelli, L., & Perinotto, M. 2003, A&A, 410, 905
Pedicelli, S., Bono, G., Lemasle, B., et al. 2009, A&A, 504, 81
Przybilla, N., Nivea, M. F., & Butler, K. 2008, ApJ, 688, L103
Ryter, Ch. E. 1996, Ap&SS, 236, 285
Savage, B. D., & Bohlin, R. C. 1979, ApJ, 229, 136
Savage, B. D., & Sembach, K. R. 1996, ARA&A, 34, 279
Snow, T. P. 1973, ApJ, 184, 135
Snow, T. P., & McCall, B. J. 2006, ARA&A, 44, 367
Snow, T. P., & Witt, A. N. 1996, ApJ, 468, L65
Snow, T. P., Destree, J. D., & Welty, D. E. 2008, ApJ, 679, 512
Snow, T. P., Rachford, B. L., & Figoski, L. 2002, ApJ, 573, 662
Sofia, U. J., & Parvahti, V. S. 2009, in Cosmic Dust – Near and Far, ed. Th. Henning et al., ASP Conf. Ser., 414, 236
Sofia, U. J., Lauroesch, J. T., Meyer, D. M., & Cartledge S. I. B. 2004, ApJ, 605, 272
Spitzer, L. 1985, ApJ, 290, L21
Spitzer, L., & Jenkins, E. B. 1975, ARA&A, 13, 133
Straižys V. 1992, Multicolor Stellar Photometry (Tucson: Pachart Publ. House)
Tabak, R. G. 1979, Ap&SS, 66, 161
Tarafdar, S. P., Prasad, S. S., & Huntres, W. T. 1983, ApJ, 267, 156
Valencic, L. A., Clayton, J. C., & Gordon, K. D. 2004, ApJ, 616, 912
Voshchinnikov, N. V. 2004, Astrophys. & Space Phys. Rev., 12, 1
Voshchinnikov, N. V., & Das, H. K. 2008, JQSRT, 109, 1527
Voshchinnikov, N. V., & Il'in, V. B. 1987, SvA Lett., 13, 157
Voshchinnikov N. V., & Il'in V. B. 1993, SvA, 37, 21
Voshchinnikov, N. V., Il'in, V. B., Henning, Th., & Dubkova, D. N. 2006, A&A, 445, 167
Wegner, W. 2002, BaltA, 11, 1
Wegner, W. 2003, AN, 324, 219
Whittet, D. C. B. 2003, Dust in the Galactic Environments, second edition (Bristol: Institute of Physics Publishing)
Whittet, D. C. B. 2010, ApJ, 710, 1009
Winkler, H. 1997, MNRAS, 287, 481
Zhukovska, S., Gail, H.-P., & Trieloff, M. 2008, A&A, 479, 453
Zubko, V. G., Dwek, E., & Arendt, R. G. 2004, ApJS, 152, 211

Pages 12 to 15 are available in the electronic edition of the journal at http://www.aanda.org

Appendix A

Table A.1. Dust phase abundances of Mg, Si, and Fe in ppm.

N (1)	Star (2)	*l* (3)	*b* (4)	Spectrum (5)	*D*, pc (6)	*E*(*B* − *V*) (7)	$[Mg/H]_d$ (8)	$[Si/H]_d$ (9)	$[Fe/H]_d$ (10)
1	HD 1383	119.02	–0.89	B1II	2702	0.47	32.56 ± 3.23	···	···
2	HD 5394	123.58	–2.15	B0IVpe	188	0.12	34.18 ± 1.98	···	30.71 ± 0.44
3	HD 12323	132.91	–5.87	ON9V	3586	0.21	34.18 ± 1.90	···	30.86 ± 0.29
4	HD 13268	133.96	–4.99	O8V	2391	0.36	33.19 ± 2.23	···	···
5	HD 13745	134.58	–4.96	O9.7IIn	1900	0.37	33.34 ± 2.44	···	30.15 ± 0.62
6	HD 14434	135.08	–3.82	O6.5V	4108	0.48	33.49 ± 2.13	···	···
7	HD 15137	137.46	+7.58	O9.5II-IIIn	3300	0.31	31.29 ± 3.37	···	30.12 ± 0.86
8	HD 18100	217.93	–62.73	B5II-III	3100	0.05	29.08 ± 4.67	16.91 ± 6.75	28.29 ± 1.53
9	HD 21856	156.32	–16.75	B1V	500	0.19	···	23.49 ± 6.51	30.69 ± 0.72
10	HD 22586	264.19	–50.36	B2III	2020	0.06	36.92 ± 1.14	···	30.02 ± 0.93
11	HD 22928	150.28	–5.77	B5III	160	0.05	39.18 ± 0.23	···	31.49 ± 0.04
12	HD 22951	158.92	–16.70	B0.5V	320	0.19	38.14 ± 1.21	···	···
13	HD 23180	160.36	–17.74	B1IVSB	219	0.29	37.71 ± 1.40	···	31.23 ± 0.30
14*	HD 23478	160.76	–17.42	B3IV	240	0.28	···	···	···
15*	HD 24190	160.39	–15.90	B2V	550	0.30	···	···	···
16	HD 24398	162.29	–16.69	B1Ib	301	0.27	36.49 ± 1.42	···	31.43 ± 0.13
17	HD 24534	163.08	–17.14	O9.5pe	590	0.59	38.54 ± 0.21	31.35 ± 0.97	31.43 ± 0.08
18	HD 24760	157.35	–10.09	B0.5IV	165	0.11	35.53 ± 1.85	···	30.95 ± 0.35
19	HD 24912	160.37	–13.10	O7V	421	0.35	35.53 ± 1.64	30.78 ± 0.49	31.33 ± 0.10
20	HD 27778	172.76	–17.39	B3V	262	0.36	38.70 ± 0.20	···	31.49 ± 0.06
21	HD 28497	208.78	–37.40	B2Vne	483	0.05	32.80 ± 3.15	23.34 ± 2.13	···
22	HD 30614	144.07	14.04	O9.5Ia	963	0.29	33.04 ± 3.04	···	30.55 ± 0.67
23	HD 34029	162.59	+4.57	G8III+G0III	13	0.01	36.08 ± 0.79	23.28 ± 2.60	29.94 ± 0.35
24	HD 34816	214.83	–26.24	B0.5IV	260	0.05	32.56 ± 3.34	···	···
25	HD 34989	194.62	–15.61	B1V	490	0.10	···	···	31.13 ± 0.38
26	HD 35149	199.16	–17.86	B1V	295	0.12	29.57 ± 4.88	25.94 ± 0.97	31.04 ± 0.25
27	HD 35715	200.09	–17.22	B2IV	370	0.04	···	···	31.08 ± 0.42
28	HD 36486	203.86	–17.74	O9.5II	281	0.08	31.86 ± 1.43	24.64 ± 1.21	30.86 ± 0.18
29	HD 36822	195.40	–12.29	B0.5IV-V	330	0.08	34.18 ± 2.75	···	31.18 ± 0.24
30	HD 36861	195.05	–12.00	O8IIIf	550	0.09	32.04 ± 3.10	···	30.95 ± 0.29
31	HD 37021	209.01	–19.38	B0V	678	0.48	38.02 ± 0.75	29.95 ± 1.53	30.98 ± 0.24
32	HD 37043	209.52	–19.58	O9III	406	0.07	32.04 ± 1.81	···	30.45 ± 0.45
33	HD 37061	208.92	–19.27	B0.5 V	476	0.53	38.63 ± 0.41	30.26 ± 0.78	31.09 ± 0.14
34	HD 37128	205.21	–17.24	B0Iab	412	0.04	33.19 ± 1.83	24.99 ± 1.88	31.02 ± 0.20
35	HD 37367	179.04	–1.03	B2 V SB	273	0.38	35.12 ± 1.94	···	···
36	HD 37468	206.82	–17.34	O9.5V	370	0.06	29.57 ± 3.22	···	30.50 ± 0.70
37	HD 37903	206.85	–16.54	B1.5V	719	0.33	38.29 ± 0.55	···	31.33 ± 0.14
38	HD 38087	207.07	–16.26	B5V	315	0.31	···	···	31.14 ± 0.16
39	HD 38666	237.29	–27.10	O9.5V	397	0.06	21.60 ± 1.72	12.45 ± 1.88	28.78 ± 0.20
40	HD 38771	214.51	–18.50	B0Iab	221	0.12	33.04 ± 1.22	···	31.05 ± 0.14
41	HD 40111	183.97	+0.84	B0.5II	480	0.18	32.21 ± 3.29	···	30.81 ± 0.60
42	HD 40893	180.09	+4.34	B0IV:	2632	0.45	33.63 ± 1.77	···	31.00 ± 0.21
43	HD 41117	189.69	–0.86	B2Ia	909	0.40	···	···	30.88 ± 0.38
44	HD 41161	164.97	+12.89	O8Vn	1400	0.21	···	···	30.81 ± 0.22
45	HD 42087	187.75	+1.77	B2.5Ib	1578	0.37	···	···	31.13 ± 0.08
46	HD 43384	187.99	+3.53	B3Ia	1100	0.58	···	···	30.53 ± 0.65
47	HD 43818	188.49	+3.87	B0II	1623	0.52	33.04 ± 1.65	···	···
48	HD 46056	206.34	–2.25	O8V(n)	1670	0.49	···	···	30.99 ± 0.10
49	HD 46202	206.31	–2.00	O9V	1670	0.47	···	···	31.28 ± 0.07
50	HD 47839	202.94	+2.20	O7Ve	313	0.07	25.67 ± 5.38	19.81 ± 3.55	···
51	HD 48915	227.23	–8.89	A1V	3	–0.01	35.63 ± 4.12	···	···
52	HD 52266	219.13	–0.68	O9IV	1735	0.26	34.55 ± 1.61	···	···
53	HD 53367	223.71	–1.90	B0IV:e	780	0.74	···	···	31.32 ± 0.12
54	HD 53975	225.68	–2.32	O7.5V	1400	0.185	30.68 ± 2.46	···	31.10 ± 0.14
55	HD 54662	224.17	–0.78	O6.5V	1220	0.26	36.71 ± 2.66	···	31.28 ± 0.18
56	HD 57060	237.82	–5.37	O7Iabfp	1870	0.14	29.80 ± 5.19	···	30.31 ± 0.63
57	HD 57061	238.18	–5.54	O9II	980	0.10	25.35 ± 4.91	23.07 ± 1.24	30.45 ± 0.39
58	HD 62542	255.92	–9.24	B5V	396	0.36	···	···	29.77 ± 1.27
59	HD 63005	242.47	–0.93	O6Vf	5200	0.28	34.67 ± 1.19	···	···
60	HD 64760	262.06	–10.42	B0.5Ib	510	0.08	30.25 ± 3.92	···	30.34 ± 0.65
61	HD 65575	266.68	–12.32	B3IVp	140	0.05	39.45 ± 0.00	···	31.47 ± 0.03

Table A.1. continued.

N (1)	Star (2)	l (3)	b (4)	Spectrum (5)	D, pc (6)	$E(B-V)$ (7)	$[\mathrm{Mg/H}]_\mathrm{d}$ (8)	$[\mathrm{Si/H}]_\mathrm{d}$ (9)	$[\mathrm{Fe/H}]_\mathrm{d}$ (10)
62	HD 65818	263.48	–10.28	B2II/IIIn	290	0.06	31.67 ± 5.56	···	···
63	HD 66788	245.43	+2.05	O8V	4200	0.20	32.72 ± 3.36	···	30.84 ± 0.33
64	HD 66811	255.98	–4.71	O5Ibnf	330	0.05	26.92 ± 2.49	13.78 ± 9.48	30.28 ± 0.29
65	HD 68273	262.80	–7.68	WC8+O9I	350	0.03	30.68 ± 4.64	21.44 ± 3.43	29.86 ± 0.57
66	HD 69106	254.52	–1.33	B0.5II	3076	0.20	34.55 ± 1.09	···	31.15 ± 0.45
67	HD 71634	273.32	–11.52	B5III	400	0.13	36.98 ± 1.53	···	···
68*	HD 72754	266.83	–5.82	B2Ia:pshe	690	0.36	···	···	···
69	HD 73882	260.18	+0.64	O8.5V	759	0.67	···	···	31.08 ± 0.19
70	HD 74375	275.82	–10.86	B1.5III	440	0.14	···	···	30.95 ± 0.54
71	HD 75309	265.86	–1.90	B2Ib/II	2924	0.28	33.77 ± 2.30	···	···
72	HD 79186	267.36	+2.25	B5Ia	980	0.40	34.79 ± 1.71	···	···
73	HD 79351	277.69	–7.37	B2IV-V	140	0.10	34.05 ± 0.00	···	···
74*	HD 88115	285.32	–5.53	B1.5IIn	3654	0.20	···	···	···
75	HD 90087	285.16	–2.13	B2/B3III	2716	0.30	···	29.80 ± 1.90	30.74 ± 0.15
76	HD 91316	234.89	+52.77	B1Iab	1754	0.04	25.35 ± 6.66	17.95 ± 4.01	···
77	HD 91597	286.86	–2.37	B7/B8IV/V	6400	0.27	33.04 ± 1.83	···	30.37 ± 0.41
78	HD 91651	286.55	–1.72	O9V:n	2964	0.28	27.21 ± 2.92	···	29.98 ± 0.36
79	HD 91824	285.70	+0.07	O7V((f))	2910	0.25	30.25 ± 2.22	···	···
80	HD 91983	285.88	+0.05	B1III	2910	0.29	30.89 ± 3.37	···	···
81	HD 92554	287.60	–2.02	O5III	6795	0.39	27.50 ± 4.53	···	29.90 ± 0.67
82	HD 93030	289.60	–4.90	B0V	140	0.04	31.29 ± 3.44	···	30.73 ± 0.32
83	HD 93205	287.57	–0.71	O3V	3187	0.38	31.48 ± 1.30	···	30.37 ± 0.24
84	HD 93222	287.74	–1.02	O7III((f))	2201	0.33	30.03 ± 1.92	···	30.25 ± 0.47
85	HD 93521	183.14	+62.15	O9Vp	1760	0.04	25.67 ± 9.98	15.42 ± 4.36	26.35 ± 2.31
86	HD 93843	228.24	–0.90	O6III	2548	0.27	31.86 ± 1.87	···	30.25 ± 0.33
87	HD 94493	289.01	–1.18	B0.5Iab	3888	0.23	30.03 ± 1.53	···	29.36 ± 0.58
88	HD 99857	294.78	–4.94	B1Ib	3058	0.33	32.72 ± 2.67	···	30.67 ± 0.30
89	HD 99890	291.75	+4.43	B0.5V:	3070	0.24	23.20 ± 6.72	···	29.51 ± 0.92
90	HD 100340	258.85	+61.23	B1V	3000	0.04	29.33 ± 3.95	26.78 ± 1.37	27.97 ± 0.88
91	HD 103779	296.85	–1.02	B0.5II	3061	0.21	30.47 ± 2.33	···	30.67 ± 0.30
92	HD 104705	297.45	–0.34	B0.5III	2082	0.28	29.57 ± 2.55	···	29.94 ± 0.54
93	HD 106490	298.23	+3.79	B2IV	110	0.06	30.25 ± 1.31	···	29.90 ± 0.23
94	HD 108248	300.13	–0.36	B0.5IV	100	0.20	22.02 ± 5.66	···	29.15 ± 0.94
95*	HD 108639	300.22	+1.95	B1III	110	0.35	···	···	···
96	HD 109399	301.71	–9.88	B1Ib	1900	0.26	33.91 ± 1.91	···	30.50 ± 0.37
97	HD 110432	301.96	–0.20	B0.5IIIe	301	0.51	···	···	31.47 ± 0.07
98	HD 111934	303.20	+2.51	B2Ib	2525	0.51	33.49 ± 2.70	···	···
99	HD 113904	304.67	–2.49	WC5+B0Ia	2660	0.21	35.12 ± 2.93	···	···
100*	HD 114886	305.52	–0.83	O9IIIn	1000	0.29	···	···	···
101*	HD 115071	305.76	+0.15	B0.5V	1200	0.44	···	···	···
102	HD 116658	316.11	+50.84	B1III-IV	80	0.14	34.29 ± 3.11	19.52 ± 8.65	29.41 ± 1.50
103	HD 116781	307.05	–0.07	B0IIIe	1492	0.34	31.86 ± 2.51	···	30.53 ± 0.48
104	HD 116852	304.88	–16.13	O9III	4832	0.21	32.04 ± 2.65	···	29.94 ± 0.48
105	HD 119608	320.35	+43.13	B1Ib	4200	0.12	29.08 ± 2.75	···	···
106	HD 121263	314.07	+14.19	B2.5IV	120	0.05	34.67 ± 0.66	···	30.77 ± 0.12
107*	HD 121968	333.97	+55.84	B1V	3800	0.15	···	···	···
108	HD 122879	312.26	+1.79	B0Ia	2265	0.36	32.04 ± 2.72	···	30.79 ± 0.36
109	HD 124314	312.67	–0.42	O6Vnf	1100	0.46	33.34 ± 1.61	···	31.02 ± 0.19
110	HD 127972	322.77	+16.67	B1.5Vne	90	0.11	22.02 ± 2.09	···	28.91 ± 0.29
111	HD 135591	320.13	–2.64	O7.5IIIf	1250	0.22	···	···	31.16 ± 0.41
112	HD 136298	331.32	+13.82	B1.5IV	210	0.07	22.82 ± 2.00	···	29.56 ± 0.32
113*	HD 137595	336.72	+18.86	B3Vn	400	0.25	···	···	···
114	HD 138690	333.19	+11.89	B2IV	130	0.07	36.17 ± 0.80	···	31.12 ± 0.06
115	HD 141637	346.10	+21.70	B2.5Vn	160	0.18	34.67 ± 2.38	30.00 ± 0.87	31.12 ± 0.43
116	HD 143018	347.21	+20.23	B1V	141	0.07	36.98 ± 2.18	27.83 ± 0.97	31.01 ± 0.26
117	HD 143118	338.77	+11.01	B2.5IV	140	0.02	36.56 ± 0.72	···	30.15 ± 0.23
118	HD 143275	350.10	+22.49	B0.3IVe	123	0.21	36.08 ± 1.08	29.65 ± 1.01	31.21 ± 0.20
119	HD 144217	353.19	+23.60	B0.5V	163	0.21	36.00 ± 0.64	29.38 ± 0.40	31.13 ± 0.35
120	HD 144470	352.76	+22.76	B1V	183	0.22	35.91 ± 1.38	···	31.26 ± 0.17
121*	HD 144965	339.04	+8.42	B2Vne	290	0.35	···	···	···
122	HD 147165	351.33	+17.00	B1IIISB,V	137	0.41	36.08 ± 3.03	30.26 ± 1.22	31.04 ± 0.52
123*	HD 147683	344.86	+10.09	B4V	280	0.39	···	···	···
124	HD 147888	353.65	+17.71	B3V:SB	195	0.51	37.85 ± 1.02	30.11 ± 1.29	31.02 ± 0.28
125	HD 147933	353.68	+17.70	B1.5V	118	0.47	38.70 ± 1.03	31.68 ± 0.23	31.44 ± 0.16

Table A.1. continued.

N (1)	Star (2)	*l* (3)	*b* (4)	Spectrum (5)	*D*, pc (6)	*E*(*B* − *V*) (7)	[Mg/H]$_d$ (8)	[Si/H]$_d$ (9)	[Fe/H]$_d$ (10)
126	HD 148184	357.93	+20.68	B1.5Ve	160	0.44	37.76 ± 1.50	···	31.28 ± 0.23
127	HD 148594	350.93	+13.94	B9:V	134	0.21	37.80 ± 0.54	···	···
128	HD 149404	340.54	+3.01	O9Ia	908	0.62	···	···	30.98 ± 0.11
129	HD 149757	6.28	+23.59	O9.5Vnn	146	0.31	37.56 ± 0.49	30.45 ± 0.40	31.43 ± 0.04
130	HD 149881	31.37	+36.23	B0.5III	2100	0.11	24.30 ± 1.40	18.27 ±11.41	28.05 ± 2.47
131	HD 151804	343.62	+1.94	O8Iab	1254	0.30	33.34 ± 3.92	···	30.77 ± 0.46
132*	HD 151805	343.20	+1.59	B1Ib	6009	0.43	···	···	···
133	HD 152236	343.03	+0.87	B1Ia	612	0.60	···	···	31.35 ± 0.14
134	HD 152590	344.84	+1.83	O7.5V	1800	0.46	34.43 ± 2.03	30.45 ± 0.79	31.08 ± 0.10
135	HD 154368	349.97	+3.22	O9Ib	1046	0.76	···	···	31.08 ± 0.26
136	HD 155806	352.59	+2.87	O7.5Ve	860	0.28	33.04 ± 3.38	···	30.94 ± 0.55
137	HD 156110	70.99	+35.91	B3Vn	720	0.03	30.89 ± 0.78	···	···
138	HD 157246	334.64	–11.48	B1Ib	348	0.06	32.88 ± 2.65	···	30.71 ± 0.44
139	HD 157857	12.97	+13.31	O7V	1902	0.43	34.18 ± 2.21	···	···
140	HD 158926	351.74	–2.21	B2IV	220	0.10	···	25.16 ± 0.95	30.15 ± 0.22
141	HD 160578	351.04	–4.72	B1.5III	142	0.08	31.67 ± 4.37	26.90 ± 2.42	30.86 ± 0.49
142	HD 164740	5.97	–1.17	O7.5V(n)	1330	0.86	···	···	31.48 ± 0.03
143	HD 165024	343.33	–13.82	B2Ib	250	0.05	33.91 ± 2.00	···	30.86 ± 0.34
144	HD 165955	357.41	–7.43	B1Vnp	1640	0.21	31.48 ± 2.25	···	···
145	HD 167264	10.46	–1.74	B0.5Ia	1514	0.30	36.08 ± 2.83	···	···
146	HD 167756	351.47	–12.30	B0.5Iab?	4230	0.07	31.67 ± 2.49	20.65 ± 4.78	30.05 ± 0.50
147	HD 168076	16.94	+0.84	O5V	1820	0.76	···	···	31.08 ± 0.45
148	HD 170740	21.06	–0.53	B2V	235	0.47	···	···	31.41 ± 0.12
149	HD 175360	12.53	–11.29	B6III	270	0.12	35.82 ± 1.18	···	···
150	HD 177989	17.81	–11.88	B2II	5021	0.22	34.18 ± 1.62	···	30.86 ± 0.27
151	HD 179406	28.23	–8.31	B3IVvar	227	0.31	···	···	31.17 ± 0.33
152	HD 184915	31.77	–13.29	B0.5IIIne	700	0.22	36.49 ± 2.44	···	···
153	HD 185418	53.60	–2.17	B0.5 V	1027	0.47	36.25 ± 1.09	···	31.21 ± 0.21
154	HD 186994	78.62	+10.06	B0III	2500	0.16	···	···	30.34 ± 0.42
155	HD 188209	80.99	+10.09	O9.5Ib	2210	0.15	···	···	30.58 ± 0.71
156	HD 190918	72.65	+2.06	WN4+O9.7Iab	2290	0.41	31.09 ± 2.25	···	···
157	HD 192035	83.33	+7.76	B0III-IVn	2800	0.35	36.25 ± 1.11	···	···
158	HD 192639	74.90	+1.48	O8V	999	0.61	34.43 ± 1.62	···	31.14 ± 0.21
159	HD 195965	85.71	+5.00	B0V	1300	0.22	34.05 ± 1.04	27.61 ± 4.47	30.87 ± 0.10
160	HD 197512	87.89	+4.63	B1V	1614	0.29	···	···	31.18 ± 0.12
161	HD 198478	85.75	+1.49	B3Ia	890	0.57	37.29 ± 1.32	···	···
162	HD 198781	99.94	+12.61	B2IV	768	0.31	35.73 ± 1.22	···	···
163*	HD 199579	87.50	–0.30	B0.5V	990	0.33	···	···	···
164	HD 201345	78.44	–9.54	O9V	2570	0.17	30.68 ± 2.75	···	···
165	HD 202347	88.22	–2.08	B1V	1300	0.19	34.90 ± 2.17	···	30.79 ± 0.34
166	HD 202904	80.98	–10.05	B2Vne	276	0.13	···	27.83 ± 4.10	30.82 ± 0.76
167	HD 203374	100.51	+8.62	B0IVpe	820	0.60	34.30 ± 2.01	28.93 ± 3.01	30.82 ± 0.31
168	HD 203532	309.46	–31.74	B5V	211	0.28	36.17 ± 3.46	···	···
169	HD 206267	99.29	+3.74	O6V	814	0.52	36.56 ± 1.15	···	31.33 ± 0.13
170	HD 206773	99.80	+3.62	B0V	597	0.45	34.30 ± 1.22	···	···
171	HD 207198	103.14	+6.99	O9II	1216	0.54	37.29 ± 0.52	···	31.32 ± 0.09
172	HD 207308	103.11	+6.82	B0.7III-IVn	1470	0.52	36.71 ± 1.00	···	31.14 ± 0.19
173	HD 207538	101.60	+4.67	O9.5V	880	0.64	36.71 ± 1.01	···	31.32 ± 0.19
174	HD 208440	104.03	+6.44	B1V	620	0.34	34.18 ± 1.98	···	···
175*	HD 208947	106.55	+9.00	B2V	500	0.19	···	···	···
176	HD 209339	104.58	+5.87	B0IV	980	0.35	33.77 ± 1.34	···	30.92 ± 0.18
177	HD 210121	56.88	–44.46	B9V	223	0.38	···	···	29.86 ± 0.88
178	HD 210809	99.85	–3.13	O9Ib	3961	0.31	31.86 ± 3.01	···	···
179	HD 210839	103.83	+2.61	O6Iab	1260	0.57	35.82 ± 1.09	···	31.13 ± 0.16
180	HD 212791	101.64	–4.30	B8	370	0.06	34.30 ± 3.98	···	···
181	HD 214680	96.65	–16.98	O9V	610	0.08	30.68 ± 4.09	···	31.22 ± 0.31
182	HD 214993	97.65	–16.18	B1.5IIIn	610	0.10	35.01 ± 2.88	···	30.05 ± 1.18
183	HD 215733	85.16	–36.35	B1II	2900	0.10	30.89 ± 5.87	21.93 ± 5.74	29.41 ± 1.04
184	HD 218376	109.96	–0.79	B1III	383	0.23	34.79 ± 4.56	···	30.73 ± 0.85
185*	HD 218915	108.06	–6.89	O9.5Iabe	3660	0.26	···	···	···
186	HD 219188	83.03	–50.17	B0.5III	1064	0.08	33.34 ± 6.30	27.72 ± 2.70	···
187	HD 220057	112.13	+0.21	B2IV	1421	0.24	36.56 ± 1.41	···	···
188	HD 224151	115.44	–4.64	B0.5II-III	1355	0.42	32.88 ± 1.70	···	30.45 ± 0.37
189	HD 224572	115.55	–6.36	B1V	340	0.19	36.00 ± 2.16	···	31.00 ± 0.53

Table A.1. continued.

N (1)	Star (2)	*l* (3)	*b* (4)	Spectrum (5)	*D*, pc (6)	$E(B-V)$ (7)	$[Mg/H]_d$ (8)	$[Si/H]_d$ (9)	$[Fe/H]_d$ (10)
190	HD 232522	130.70	–6.71	B1II	5438	0.21	31.48 ± 1.94	· · ·	· · ·
191	HD 303308	287.59	–0.61	O3V	3631	0.45	32.56 ± 2.16	· · ·	30.28 ± 0.41
192	HD 308813	294.79	–1.61	O9.5V	2398	0.28	32.56 ± 2.08	· · ·	· · ·
193	BD +35 4258	77.19	–4.74	B0.5 Vn	3093	0.25	32.72 ± 2.97	· · ·	30.22 ± 0.64
194*	BD +53 2820	101.24	–1.69	B0IV:n	4506	0.37	· · ·	· · ·	· · ·
195	CPD -59 2603	287.59	–0.69	O7V	2630	0.46	32.72 ± 1.56	18.91 ± 3.64	30.37 ± 0.32
196*	CPD -69 1743	303.71	–7.35	B1Vn	4700	0.30	· · ·	· · ·	· · ·

Notes. Dust phase abundances are calculated as difference between solar abundances ($[Mg/H]_\odot$ = 39.8 ppm, $[Si/H]_\odot$ = 32.4 ppm, $[Fe/H]_\odot$ = 31.6 ppm, Asplund et al. 2009) and gas phase abundances. (*) For these stars only gas phase abundances of O are measured.